INTERNATIONAL JOURNAL FOR NUMERICAL AND ANALYTICAL METHODS IN GEOMECHANICS, VOL. 19, 195–218 (1995)

BOUNDARY ELEMENT ANALYSIS OF STRESSES IN AN AXISYMMETRIC SOIL MASS UNDERGOING CONSOLIDATION

MANOJ B. CHOPRA*

Department of Civil and Environmental Engineering, University of Central Florida, Orlando, FL 32816, USA

AND

GARY F. DARGUSH

Department of Civil Engineering, State University of New York at Buffalo, Buffalo, NY 14260, USA

SUMMARY

A time domain boundary element method (BEM) for evaluating stresses in an axisymmetric soil mass undergoing consolidation has been developed. Previous BEM work on axisymmetric poroelasticity for boundary displacements and pore pressures is extended to permit the computation of stresses at both boundary and interior points. The stress formulation preserves the surface-only discretization.

The boundary displacement integral equation is progressively differentiated to obtain the related stress and strain integral equations. Explicit expressions for the steady-state axisymmetric fundamental solutions are derived in this process. The transient components of the integrands are obtained directly from the transformation of the three-dimensional kernels into a cylindrical system. Numerical implementation of these integral equations is carried out within a general purpose BEM computer code and several illustrative examples are presented to validate the method.

INTRODUCTION

Within the realm of geotechnical engineering, it is often of great importance to determine the stresses in a soil mass subjected to quasistatic loading. The present paper aims to develop a numerical technique for the evaluation of these stresses within a poroelastic body. In addition, a number of such problems in practice involve axisymmetric geometries. The reduction in dimensionality of the problem leads to substantial benefits in computational time and effort.

Biot[1] was the first to develop a general three-dimensional theory of soil consolidation. However, after the birth of this theory, only a few analytical solutions to the differential equations exist in the literature (e.g. References 2 and 3). In general, for solving realistic practical applications, numerical methods such as the finite element method (FEM) and the boundary element method (BEM) have been utilized. Initially, FEM was applied to the field of poroelasticity by Sandhu and Wilson[4] and Ghaboussi and Wilson.[5] This was followed by several other workers using FEM. More recently, BEM has emerged as an attractive alternative to FEM due to a surface-only solution methodology based upon the boundary integral equations. The increased popularity of BEM is evidenced in its application to a number of fields including soil consolidation.

CCC 0363–9061/95/030195–24

Received 1 December 1993
Revised 11 August 1994

In particular, the first application of BEM to quasistatic soil consolidation was done by Banerjee and Butterfield[6] via a volume-based staggered approach to the coupled equations. In this approach, the transient flow equations were first solved at each time step, followed by a deformation analysis for that instant. Aramaki and Yasuhara[7] utilized this volume-based approach for solving axisymmetric problems. On the other hand, Cheng and Liggett[8,9] solved two-dimensional problems of soil consolidation by employing Laplace domain fundamental solutions.

Dargush and Banerjee[10] have presented a time domain boundary-only BEM for soil consolidation in two and three dimensions based upon the fundamental solutions of Nowacki,[11] Cleary[12] and Rudnicki.[13] This formulation was the first to suitably verify the solutions with closed-form solutions and was sufficiently general to serve as a practical tool. Subsequently, Dargush and Banerjee[14] extended this formulation to axisymmetric problems. The method was, however, restricted to the computation of primary surface quantities only. The present work is based upon this method and aims to extend it to enable the determination of stresses and strains at any point, either on the surface or in the interior, of the consolidating soil mass. The primary advantage of a boundary-only discretization is preserved in the present implementation. In fact, only a line representing the generator of the axisymmetric solid needs to be modelled. The entire formulation is carried out exclusively in time domain leading to very accurate results.

The next section discusses the coupled differential equations that govern Biot's theory of soil consolidation in three dimensions. Next, the integral formulations for displacements and stresses for the axisymmetric case are presented. Based upon the previous work, the three-dimensional fundamental solutions are decomposed into the steady and non-steady parts and then are suitably transformed into their axisymmetric counterparts. This is followed by progressive differentiation of the boundary displacement integral equation to obtain the integral formulations for stress and strain at an interior point within the soil mass. The fundamental solutions associated with the interior stress and strain behaviour are derived in the process. Surface stress is determined directly in terms of primary boundary variables, using the well-established method used in elastostatics.

Spatial and temporal discretizations are carried out to render the exact integral formulations suitable for practical analysis. Some illustrative examples of stress analysis are presented to establish the accuracy and validity of the present development. Standard indicial notation is used wherein a comma represents differentiation in space, a superposed dot a time derivative and repeated indices are summed.

GOVERNING EQUATIONS

Terzaghi[15] first laid down the theoretical foundation to soil consolidation with the introduction of the effective stress concept. Subsequently, Biot[1] generalized Terzaghi's one-dimensional theory for saturated soils to the three-dimensional, partial saturation case. The effective stress concept, in generalized co-ordinates, may be expressed as

$$\sigma_{ij} = \sigma'_{ij} - \delta_{ij}\beta u_p \tag{1a}$$

where σ_{ij} is the total stress state, σ'_{ij} is the effective stress state, u_p is the excess pore water pressure, δ_{ij} is the Kronecker delta and β is a dimensionless material parameter relating the compressibilities of the solid and fluid constituents and may be expressed as (e.g. Reference 16)

$$\beta = 1 - \frac{K}{K'_s} \tag{1b}$$

where $K = \lambda + \frac{2}{3}\mu$ is the bulk modulus of the soil under drained conditions and K_s' is an arbitrary constant which reduces to the bulk modulus of the solid skeleton under certain specific conditions. The constants λ and μ are Lame's elastic constants under drained conditions.

The governing equations for coupled quasistatic poroelasticity (CQP) may be written as[15]

$$(\lambda + \mu)u_{j,ij} + \mu u_{i,jj} - \beta u_{p,i} + b_i = 0 \tag{2a}$$

$$\kappa u_{p,jj} - \alpha \dot{u}_p - \beta \dot{u}_{j,j} + \psi = 0 \tag{2b}$$

where κ is the permeability and $\alpha = \beta^2/(\lambda_u - \lambda)$. In equation (2), u_i denotes the displacement vector, b_i is the body force vector per unit volume, ψ is the rate of fluid supply per unit volume and λ_u is the undrained elastic modulus.

In order to establish the undrained constants, it is desirable to determine the undrained bulk modulus (K_u), which can be measured with ease. This is done through the use of the undrained Poisson's ratio, ν_u, which is given by

$$\nu_u = \frac{3K_u + 2\mu}{6K_u + 2\mu} \tag{3}$$

Thus, the constants β and α can now be expressed in terms of the undrained bulk modulus as

$$\beta = \frac{1}{B}\left[1 - \frac{K}{K_u}\right] \tag{4a}$$

$$\alpha = \frac{\beta}{K_u B} \tag{4b}$$

where B is the well-known Skempton's coefficient of pore pressure.

The material parameter determining the rate of diffusion is called the coefficient of consolidation, c_v, and is given by

$$c_v = \frac{2\mu\kappa(1 - \nu)}{(1 - 2\nu)}\left[\frac{B^2}{9}\frac{(1 + \nu_u)^2(1 - 2\nu)}{(\nu_u - \nu)(1 - \nu_u)}\right] \tag{5}$$

BOUNDARY INTEGRAL FORMULATION FOR AXISYMMETRY

In the absence of body forces and sources and under zero initial conditions and by utilizing the analogous thermoelastic reciprocal theorem,[17] equation (1) leads to the following boundary integral equation:[14]

$$c_{\beta\alpha}(\xi)u_\beta(\xi, \tau) = \int_S [g_{\beta\alpha}(X; \xi, \tau) * t_\beta(X, \tau) - f_{\beta\alpha}(X; \xi, \tau) * u_\beta(X, \tau)]\, dS(X) \tag{6}$$

where the generalized displacements and tractions are defined by

$$u_\beta = \{u_1 \;\; u_2 \;\; u_3 \;\; u_p\}^T \tag{7a}$$

$$t_\beta = \{t_1 \;\; t_2 \;\; t_3 \;\; q\}^T \tag{7b}$$

in which t_i are tractions and q is the flux. Greek indices are used to denote generalized co-ordinates varying from one to four in three dimensions. The tensor $c_{\beta\alpha}$ depends upon the local geometry at ξ and reduces to the delta function in generalized co-ordinates, $\delta_{\beta\alpha}$, for a point inside the surface S. The asterisk ($*$) denotes a Riemann convolution integral in time which implies, for

instance,

$$f_{\beta\alpha} * u_\beta = \int_0^t [f_{\beta\alpha}(X, t-\tau)u_\beta(X,\tau)]\,\mathrm{d}\tau = \int_0^t [f_{\beta\alpha}(X,\tau)u_\beta(X, t-\tau)]\,\mathrm{d}\tau \tag{7c}$$

The kernel functions, $g_{\beta\alpha}$ and $f_{\beta\alpha}$, are derived from the infinite space fundamental solutions for instantaneous point force and source for three-dimensional poroelasticity.[11-13]

The axisymmetric geometry is modelled using a cylindrical co-ordinate system (r, θ, z). The generalized co-ordinates, u_β and t_β, are transformed into this cylindrical system. Under purely axisymmetric conditions, the problem becomes independent of the circumferential degree of freedom and $u_\theta = 0$; $t_\theta = 0$. The kernel functions are then integrated from 0 to 2π in the circumferential direction. It must be noted that while the steady-state kernels, $G_{\beta\alpha}$ and $F_{\beta\alpha}$, can be integrated analytically in terms of elliptic integrals, the transient components have to be handled numerically. Thus, upon isolating the steady and non-steady parts of the kernels and subsequent transformation and integration, the boundary integral equation (6) may be written as[14]

$$\begin{aligned}\bar{c}_{\beta\alpha}(\xi)\bar{u}_\beta(\xi,\tau) = &\int_C [\hat{G}_{\beta\alpha}(X;\xi)\bar{t}_\beta(X,\tau) - \hat{F}_{\beta\alpha}(X;\xi)\bar{u}_\beta(X,\tau)]\,\mathrm{d}C \\ &+ \int_C \int_0^{2\pi} [\bar{g}^{\mathrm{tr}}_{\beta\alpha}(X;\xi,\tau) * \bar{t}_\beta(X,\tau) - \bar{f}^{\mathrm{tr}}_{\beta\alpha}(X;\xi,\tau) * \bar{u}_\beta(X,\tau)]\,\mathrm{d}\theta\,\mathrm{d}C\end{aligned} \tag{8}$$

where

$$\bar{u}_\alpha = T_{\beta\alpha}u_\beta = \{u_r \;\; u_z \;\; u_{\mathrm{p}}\}^{\mathrm{T}} \tag{9a}$$

$$\bar{t}_\alpha = T_{\beta\alpha}t_\beta = \{t_r \;\; t_z \;\; q\}^{\mathrm{T}} \tag{9b}$$

where $T_{\beta\alpha}$ is the transformation tensor and the kernel functions are suitably transformed into the cylindrical system as described in Dargush and Banerjee.[14] The various kernels are defined as

$$g_{\beta\alpha} = G_{\beta\alpha} + g^{\mathrm{tr}}_{\beta\alpha} \tag{10a}$$

$$f_{\beta\alpha} = F_{\beta\alpha} + f^{\mathrm{tr}}_{\beta\alpha} \tag{10b}$$

$$\hat{G}_{\beta\alpha} = \int_0^{2\pi} \bar{G}_{\beta\alpha}\,\mathrm{d}\theta \tag{10c}$$

$$\hat{F}_{\beta\alpha} = \int_0^{2\pi} \bar{F}_{\beta\alpha}\,\mathrm{d}\theta \tag{10d}$$

where

$$\bar{G}_{\beta\alpha} = \tilde{T}_{\gamma\beta}G_{\gamma\delta}T_{\delta\alpha}r(X) \tag{11a}$$

$$\bar{F}_{\beta\alpha} = \tilde{T}_{\gamma\beta}F_{\gamma\delta}T_{\delta\alpha}r(X) \tag{11b}$$

$$\bar{g}^{\mathrm{tr}}_{\beta\alpha} = \tilde{T}_{\gamma\beta}g^{\mathrm{tr}}_{\gamma\delta}T_{\delta\alpha}r(X) \tag{11c}$$

$$\bar{f}^{\mathrm{tr}}_{\beta\alpha} = \tilde{T}_{\gamma\beta}f^{\mathrm{tr}}_{\gamma\delta}T_{\delta\alpha}r(X) \tag{11d}$$

$$\bar{c}_{\beta\alpha} = \tilde{T}_{\gamma\beta}c_{\gamma\delta}T_{\delta\alpha} \tag{11e}$$

with $T_{\delta\alpha}$ as the transformation matrix evaluated at X and $\tilde{T}_{\gamma\beta}$ as the transformation evaluated at ξ which reduces to an identity matrix, since the z-axes of the two systems coincide and $\theta = 0$ at ξ. In equation (11), $r(X)$ is the radial co-ordinate of the point X.

The components $\hat{G}_{rr}$, $\hat{G}_{rz}$, $\hat{G}_{zr}$, $\hat{G}_{zz}$, $\hat{F}_{rr}$, $\hat{F}_{rz}$, $\hat{F}_{zr}$ and $\hat{F}_{zz}$ of the steady-state kernels are identical to the axisymmetric elasticity kernels.[18] In addition, the components $\hat{G}_{pp}$ and $\hat{F}_{pp}$ are the well-known axisymmetric potential flow kernels found in Banerjee and Butterfield.[6] The entire steady-state boundary kernel is coupled for the poroelastic case and is provided by Dargush and Banerjee[14] in detail.

The strain at any interior point is now determined by using equation (8) in the strain – displacement relations and setting $\bar{c}_{\beta\alpha} = \delta_{\beta\alpha}$. It may be expressed as

$$\bar{\varepsilon}_{ij}(\xi,\tau) = \int_C [\hat{G}^{\varepsilon}_{\beta ij}(X;\xi)\bar{t}_\beta(X,\tau) - \hat{F}^{\varepsilon}_{\beta ij}(X;\xi)\bar{u}_\beta(X,\tau)]\,\mathrm{d}C + \int_C \int_0^{2\pi} [{}^{\mathrm{tr}}\bar{g}^{\varepsilon}_{\beta ij}(X;\xi,\tau) * \bar{t}_\beta(X,\tau) - {}^{\mathrm{tr}}\bar{f}^{\varepsilon}_{\beta ij}(X;\xi,\tau) * \bar{u}_\beta(X,\tau)]\,\mathrm{d}\theta\,\mathrm{d}C \tag{12}$$

where the interior strain kernels can be evaluated as

$$\hat{G}^{\varepsilon}_{\beta ij} = \tfrac{1}{2}[\hat{G}_{\beta i,j} + \hat{G}_{\beta j,i}] \tag{13a}$$

$$\hat{F}^{\varepsilon}_{\beta ij} = \tfrac{1}{2}[\hat{F}_{\beta i,j} + \hat{F}_{\beta j,i}] \tag{13b}$$

$${}^{\mathrm{tr}}\bar{g}^{\varepsilon}_{\beta ij} = \tfrac{1}{2}[\bar{g}^{\mathrm{tr}}_{\beta i,j} + \bar{g}^{\mathrm{tr}}_{\beta j,i}] \tag{13c}$$

$${}^{\mathrm{tr}}\bar{f}^{\varepsilon}_{\beta ij} = \tfrac{1}{2}[\bar{f}^{\mathrm{tr}}_{\beta i,j} + \bar{f}^{\mathrm{tr}}_{\beta j,i}] \tag{13d}$$

Using the elastic constitutive tensor in terms of effective stresses in cylindrical form, the effective stress at any point ξ in the interior of surface S may be written as

$$\bar{\sigma}'_{ij}(\xi,\tau) = \int_C [\hat{G}^{\sigma}_{\beta ij}(X;\xi)\bar{t}_\beta(X,\tau) - \hat{F}^{\sigma}_{\beta ij}(X;\xi)\bar{u}_\beta(X,\tau)]\,\mathrm{d}C + \int_C \int_0^{2\pi} [{}^{\mathrm{tr}}\bar{g}^{\sigma}_{\beta ij}(X;\xi,\tau) * \bar{t}_\beta(X,\tau) - {}^{\mathrm{tr}}\bar{f}^{\sigma}_{\beta ij}(X;\xi,\tau) * \bar{u}_\beta(X,\tau)]\,\mathrm{d}\theta\,\mathrm{d}C \tag{14}$$

Once again, the interior stress kernels $\hat{G}^{\sigma}_{kij}$ and $\hat{F}^{\sigma}_{kij}$ are identical to those encountered in steady-state axisymmetric elasticity. The remaining kernels such as $\hat{G}^{\sigma}_{pij}$, $\hat{F}^{\sigma}_{pij}$ as well as the entire transient kernels, ${}^{\mathrm{tr}}\bar{g}^{\sigma}_{\beta ij}$ and ${}^{\mathrm{tr}}\bar{f}^{\sigma}_{\beta ij}$, have been derived in the poroelastic context as a part of the present development.

The steady-state coupled axisymmetric kernels, $\hat{G}^{\sigma}_{pij}$ and $\hat{F}^{\sigma}_{pij}$, for interior stress are presented in the Appendix. The transient kernels are explained in further detail later in the paper. Equations (8), (12) and (14) are all exact statements without any approximations. In principle, if these equations are written for every point on the boundary starting from time zero to the present time and solved simultaneously, exact solutions to the desired boundary value problem can be obtained. In reality, however, the analysis must be restricted to a finite number of equations at some discrete time intervals. This is done by using discretization schemes as discussed in the next section.

NUMERICAL IMPLEMENTATION

The application of the integral equations for boundary displacements and interior stresses to the problems of practical engineering interest requires discretization in both time and space. Dargush and Banerjee[10,14] discuss the numerical implementation schemes for the axisymmetric analysis from the viewpoint of boundary displacements. Consequently, the present discussion is confined

to the extension of the different features of the numerical algorithm for the evaluation of stresses. It may be noted that all past information is retained in the numerical discretization schemes and no volume integration is required to be performed. This preserves the attractive boundary-only feature of BEM.

For the temporal discretization, the time interval from zero to t can be divided into N equal increments of duration Δt. Thus, the convolution integrals in (14) with limits from zero to t can be represented as a sum of N integrals using a piecewise constant time marching scheme. The primary variables, $\bar{u}_\beta$ and $\bar{t}_\beta$, are assumed to remain constant within each time increment Δt. This assumption is found to be sufficiently accurate and more computationally efficient than the use of higher-order variation for time for diffusive system of equations. In comparison, higher-order time variation is typically required for a hyperbolic system such as elastodynamics.[19] These variables can then be brought outside the integrals in (14) and the effective stress equation may be written, for the Nth time increment as

$$(\bar{\sigma}')_{ij}^{N}(\xi) = \int_C [\hat{G}^{\sigma}_{\beta ij}(X;\xi)\bar{t}_\beta^{N}(X) - \hat{F}^{\sigma}_{\beta ij}(X;\xi)\bar{u}_\beta^{N}(X)]\,\mathrm{d}C + \sum_{n=1}^{N}\left\{\int_C [\hat{G}^{\sigma;N-n+1}_{\beta ij}(X;\xi)\bar{t}_\beta^{n}(X) - \hat{F}^{\sigma;N-n+1}_{\beta ij}(X;\xi)\bar{u}_\beta^{n}(X)]\,\mathrm{d}C\right\} \tag{15}$$

where the interior stress transient kernels are

$$\hat{G}^{\sigma;N-n+1}_{\beta ij} = \int_0^{2\pi} \bar{G}^{\sigma;N-n+1}_{\beta ij}\,\mathrm{d}\theta \tag{16a}$$

$$\hat{F}^{\sigma;N-n+1}_{\beta ij} = \int_0^{2\pi} \bar{F}^{\sigma;N-n+1}_{\beta ij}\,\mathrm{d}\theta \tag{16b}$$

with

$$\hat{G}^{\sigma;N-n+1}_{\beta ij}(X;\xi) = G^{\sigma;N-n+1}_{\gamma ij} T_{\gamma\beta}\, r(X) \tag{17a}$$

$$\hat{F}^{\sigma;N-n+1}_{\beta ij}(X;\xi) = F^{\sigma;N-n+1}_{\gamma ij} T_{\gamma\beta}\, r(X) \tag{17b}$$

The resulting transient stress kernels are provided in the appendix. Similar to the case of the boundary equation,[14] the circumferential integration in (16) cannot be done in closed form and requires the use of Gaussian quadrature formulae. Higher-order Gaussian rules and self-adaptive integration[20] are employed to conduct this circumferential integration.

The next step is the discretization of the curve C in the r–z plane to enable numerical evaluation of the line integrals in equation (15). The discretization approach taken by Dargush and Banerjee[14] based upon the work of Henry *et al.*[18] is utilized for the present implementation. Three-noded quadratic surface elements are used with either linear or quadratic functional variation. The strongly singular components of the static boundary kernels are evaluated using the rigid body and the inflation mode techniques.[14,18] Since the stress equation is written at the interior point, the entire steady-state stress kernels, $\hat{G}^{\sigma}_{\beta ij}$ and $\hat{F}^{\sigma}_{\beta ij}$, are non-singular and well-behaved. However, special care needs to be taken in the numerical evaluation of these kernels, if the field point and the load point come in close proximity. The singularity in axisymmetric kernels when the load point falls on the axis of symmetry ($\xi_r = 0$) is circumvented by simply

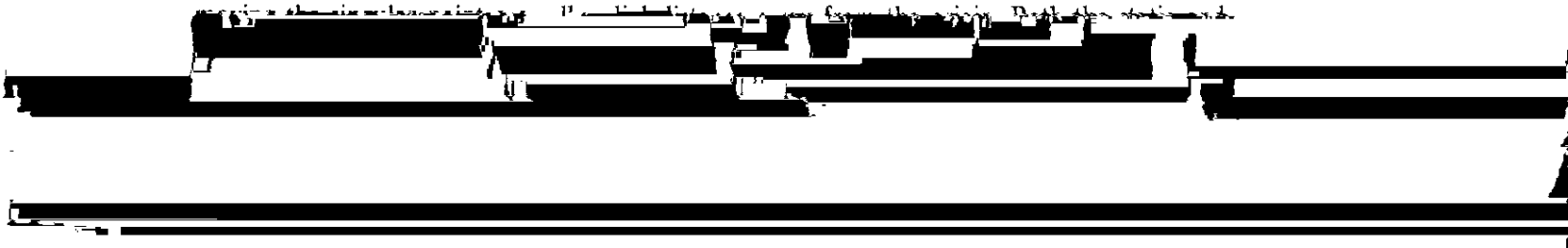

transient components are evaluated at the first time step. Only spatial integration of the transient

Next, a spatially discretized form of the boundary integral equation is written for each boundary node and the method of collocation is used to assemble a system of algebraic equations. This system of equations is solved for the unknown generalized variables at a particular time step. Further details of the assembly and solution process for the boundary equations are presented in Reference 10. Upon solving the boundary equations for $\{\bar{u}^N\}$ and $\{\bar{t}^N\}$, the stress response at any point in the interior of the body is computed by simple substitution into the collocated form of the stress equation (15). The kernels exhibit strong singularities if ξ is taken to the surface. The boundary stresses are instead determined as a result of a limiting process involving the tangential derivatives of the displacement and traction fields along with Hooke's law. This technique is detailed in Cruse and Vanburen[21] and Rizzo and Shippy[22] for elastostatics. In the poroelastic case, the following relations may be used for boundary stress calculation:

$$(\bar{\sigma}')^N_{ij}(\xi) n_j(\xi) = N_\omega(\zeta) \bar{t}^N_{i\omega} \tag{18a}$$

$$(\bar{\sigma}')^N_{ij}(\xi) - \frac{D^e_{ijkl}}{2}[\bar{u}^N_{k,l}(\xi) - \bar{u}^N_{l,k}(\xi)] = -\beta \delta_{ij} N_\omega(\zeta) \bar{u}^N_{p\omega} \tag{18b}$$

$$\bar{u}^N_{i,j}(\xi) \frac{\partial x_j}{\partial \zeta} = \frac{\partial N_\omega}{\partial \zeta} \bar{u}^N_{i\omega} \tag{18c}$$

where N_ω is the shape function employed, $\bar{t}^N_{i\omega}$ is the nodal traction, $\bar{u}^N_{p\omega}$ is the nodal pore pressure and D^e_{ijkl} is the elastic constitutive tensor. The set of equations (18) can be solved for $\bar{\sigma}^N_{ij}(\xi)$ and $\bar{u}^N_{i,j}(\xi)$ in terms of the known nodal quantities.

The poroelastic BEM formulation for the evaluation of stresses at any point in the soil mass was implemented within a general-purpose computer code (GPBEST). The capability of this code to analyse substructured problems offers additional advantages and permits the analysis of bodies with multiple materials and intricate geometries. Some numerical applications of this formulation are discussed in the following section.

NUMERICAL APPLICATIONS

Consolidation of a solid sphere

As a first example of poroelasticity using the axisymmetric BEM formulation, consider the consolidation of a saturated solid sphere of soil subjected to hydrostatic pressure. Based upon the theories of Terzaghi[13] and subsequently Biot,[1,23] the first quasistatic analytical solutions to this problem were presented by Cryer.[24] Closed-form solutions for the surface displacement and the pore pressure change at the centre of the sphere were developed in the above reference and are discussed below. In the previous work by Dargush and Banerjee,[14] this problem was studied for the evaluation of the displacement and pore pressure responses. In all cases, very good correlation was obtained between Cryer's solutions and BEM results. In the present paper, this investigation is extended to the computation of stresses in the soil. It is notable that Cryer's formulations are constructed in terms of non-dimensional quantities. Hence, by definition,

$$T = c_v t / a^2$$

$$U_p = u_p / P$$

$$R = r/a$$

$$\mu_c = \frac{\mu}{2\mu + \lambda}, \qquad \lambda_c = \frac{\lambda}{2\mu + \lambda} \tag{19}$$

where a is the radius of the sphere, c_v is the coefficient of consolidation, u_p is the pore pressure, P is the applied load intensity, t is the time and r is the radial distance from the centre. Cryer[24] has presented solutions for the non-dimensional displacement of the surface at time T (i.e. $U_R(1, T)$) and the non-dimensional pore pressure at the centre of the sphere (i.e. $U_p(0, T)$).

The displacement solutions may be generalized for any radius R as

$$U_R(R, T) = R + \sum_{n=1}^{\infty} \frac{8\mu_c(3 - 4\mu_c)}{R^2}\left[\frac{R\sqrt{s_n}\cos(R\sqrt{s_n}) - \sin(R\sqrt{s_n})\exp(-s_nT)}{s_n(s_n - 12\mu_c + 16\mu_c^2)\sin(R\sqrt{s_n})}\right] \tag{20}$$

which reduces to Cryer's expression for $U_R(1, t)$ by setting $R = 1$. Next, the effective radial stress (σ'_R) at any radius R may be derived as

$$\sigma'_R(R, T) = \frac{P}{(3 - 4\mu_c)}\left[\frac{dU_R}{dR} + (2 - 4\mu_c)\frac{U_R}{R}\right] \tag{21}$$

In particular, the effective radial stress at the centre of the sphere (i.e. $R = 0$) is given by

$$\sigma'_R(0, T) = P\left[1 + \sum_{n=1}^{\infty} \bar{f}(\mu_c, s_n, T)\frac{s_n\sqrt{s_n}}{3}\right] \tag{22a}$$

where

$$\bar{f}(\mu_c, s_n, T) = \frac{8\mu_c(3 - 4\mu_c)\exp(-s_nT)}{s_n(s_n - 12\mu_c + 16\mu_c^2)\sin\sqrt{s_n}} \tag{22b}$$

Similar to the previous study, three different cases, corresponding to $\mu_c = 0, 0{\cdot}25$ and $0{\cdot}5$ are considered. However, $\mu_c = 0$ implies incompressible behaviour leading to $\nu = 0{\cdot}5$. This then requires special numerical treatment for axisymmetric analyses.[25] Consequently, in the present work, a numerical convergence study was conducted and a value of $\mu_c = 0{\cdot}01$ was found suitable in approximating the condition $\mu_c = 0$. The material constants for this problem corresponding each of the above cases are tabulated below:

μ_c	ν	E
0·5	0·0	1·0
0·25	0·333	0·666
0·01	0·495	0·0299

The fluid properties, namely, the permeability, the density of the fluid and the undrained Poisson's ratio, are all selected as unity. The axisymmetric BEM mesh is shown in Figure 1, consisting of four, three-noded elements. In addition, a few interior points are placed within the sphere to monitor the stresses and pore pressures in the interior. The size of the time step is selected as 0·00625 based on the diffusivity and the element length. The results obtained from the present analysis using GPBEST are compared to the exact solutions discussed earlier. Figure 2 displays the BEM results for the variation of the radial displacement at the surface ($R = 1$) with time for $\mu_c = 0, 0{\cdot}25, 0{\cdot}50$. This solution is identical to the one obtained by Dargush and Banerjee[14] and is presented here for the sake of completeness and better understanding of the problem. Cryer's solution for this case is also plotted. The agreement between the solutions is excellent. In Figure 3, the relationship between the pore pressure at the centre of the sphere and

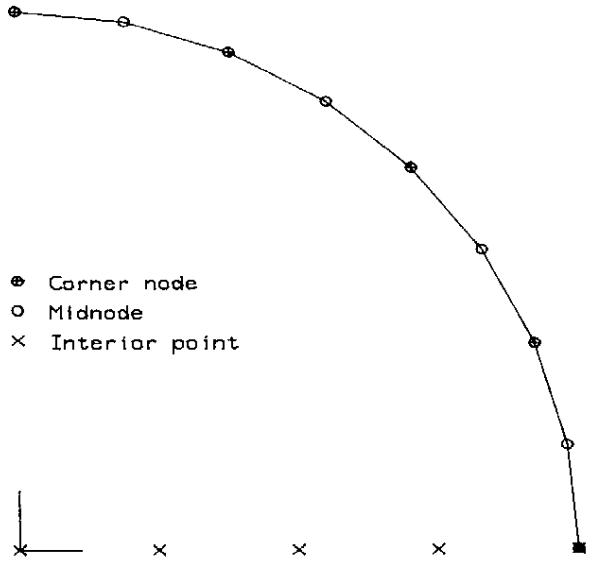

Figure 1. Consolidation of a solid sphere — boundary element model

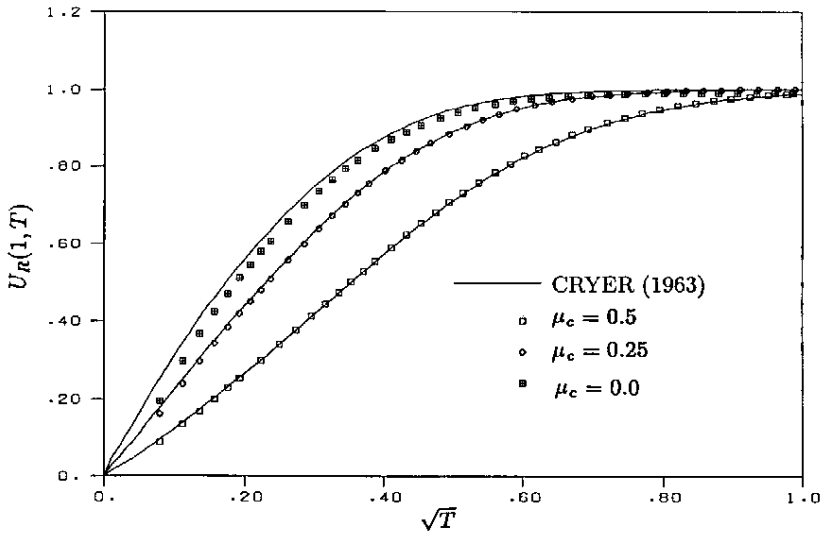

Figure 2. Variation of radial displacement at surface of the sphere with time for μ_c = 0·0, 0·25 and 0·5

the surface radial displacement for the values of μ_c is plotted in a manner similar to the results in Cryer's paper. Once again, very good correlation is obtained.

The focus is then shifted to the computation of the effective radial stress at the centre of the sphere. The variations of the effective radial stress and the pore pressure are discussed together

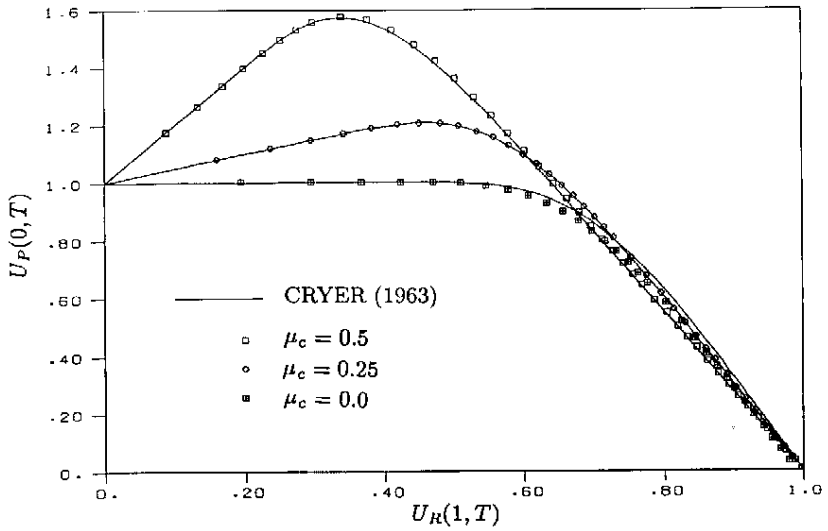

Figure 3. Relationship between pore pressure at the centre of the sphere and the radial displacement of the surface for $\mu_c = 0{\cdot}0$, $0{\cdot}25$ and $0{\cdot}5$

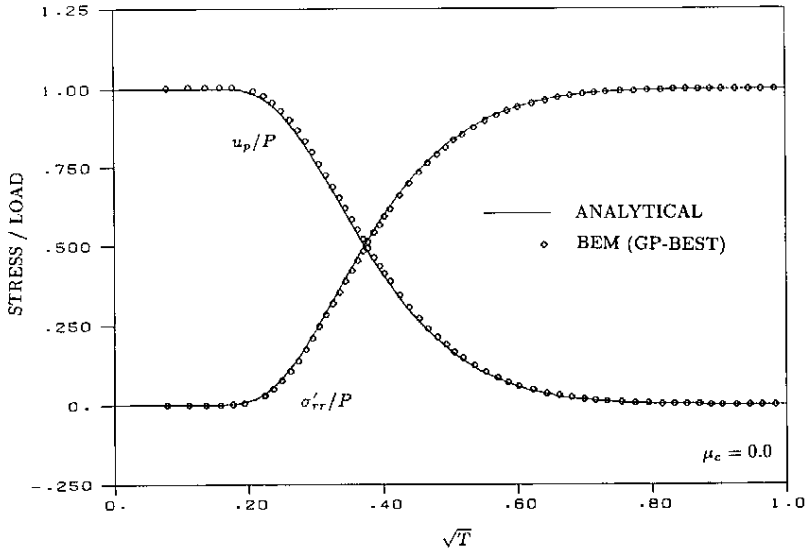

Figure 4. Variation of effective radial stress with time for $\mu_c = 0{\cdot}0$

showing the salient features of the consolidation phenomenon. Initially, the entire applied hydrostatic pressure is absorbed by an increase in pore pressure. However, with time, the pore pressure gradually diminishes while the effective stress simultaneously increases.

Ultimately, at very large times, the pore pressure is completely decayed while the effective stress becomes equal to the hydrostatic pressure on the sphere. For the incompressible case, i.e.,

$\mu_c = 0{\cdot}0$, the two stresses (u_p and σ'_{rr}) are complementary at all times, as seen in Figure 4, and the total stress is always equal to the pressure applied. However, for cases with compressible soil skeletons, the pore pressure initially rises before decaying to zero. This is evident from Figure 5 for $\mu_c = 0{\cdot}25$ and Figure 6 for $\mu_c = 0{\cdot}50$. On the other hand, the effective stress invariably rises from initial zero value to equal the applied pressure at steady state. The increase of pore pressure,

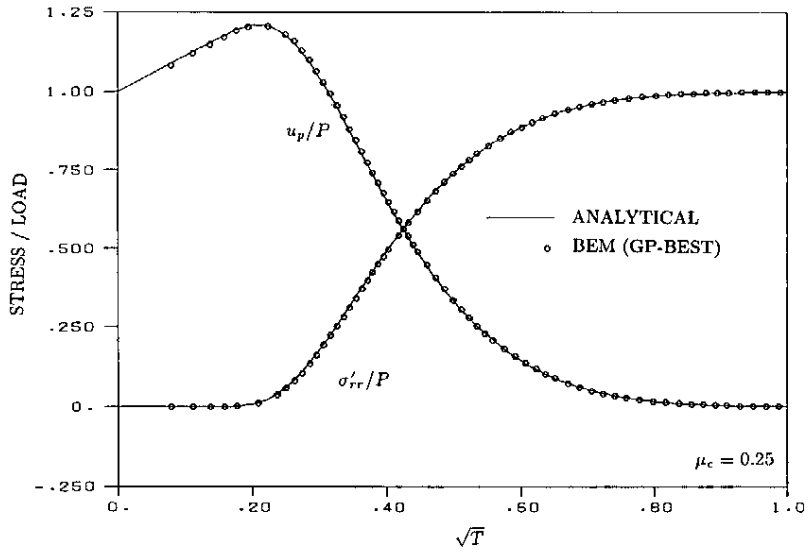

Figure 5. Variation of effective radial stress with time for $\mu_c = 0{\cdot}25$

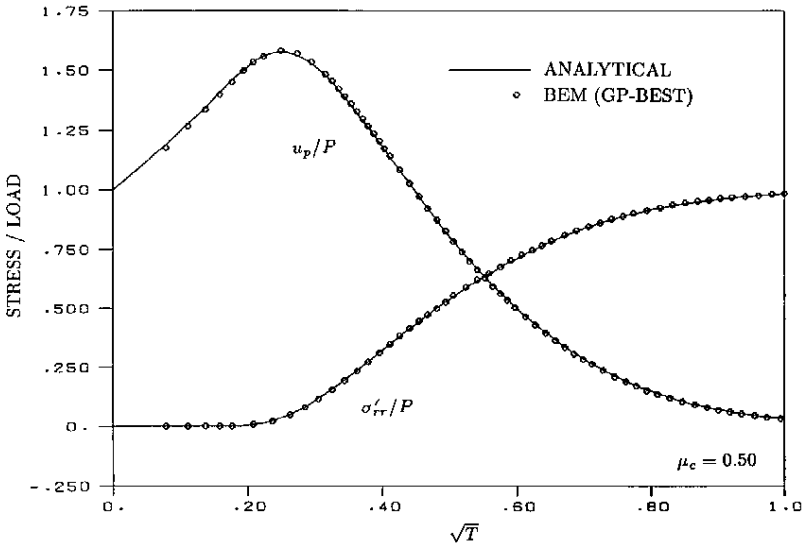

Figure 6. Variation of effective radial stress with time for $\mu_c = 0{\cdot}5$

also observed in Figure 3, is a peculiarity of Biot's theory of consolidation of compressible soils and was first noted by Cryer.[24] It is clear from Figures 4–6 that the present BEM formulation provides a good prediction of the exact solutions for the stress response in this quasistatic poroelastic problem.

Stresses due to the withdrawal of pore fluid

The withdrawal of pore fluid from a soil leads to the subsidence of the ground surface. The removal of pore fluid may be required for several purposes, namely, the pumping of water, oil or natural gas, the lowering of the ground water table to allow excavations, or the reduction of excessive pore water pressure in the ground. The problem of subsidence as a result of pumping of water or some other fluid from the ground has been examined in detail by Small and Booker[26] and Booker and Carter,[2,3] who have derived analytical or semi-analytical solutions for both the steady state and the transient cases. Recently, Hsi *et al.*[27] presented a finite element solution to the problem of pumping-induced subsidence by also accounting for the effects of the drawdown of the water table. In the present study, this problem is studied with particular emphasis on the build-up of stresses around the sink as a result of the pumping process.

The removal of pore fluid leads to the reduction of pore pressures in the vicinity of the sink. This in turn leads to an increase in the compressive effective stresses in the soil. The consolidation caused by this reduction of pore pressure and increase in effective stress leads to subsidence of the ground surface. Booker and Carter[2,3] have analysed this problem in detail and present closed-form solutions for the long-term subsidence and the pore pressure response at steady state. In addition, these authors also present a transient solution to this problem considering the soil to be isotropic and elastic but with anisotropic flow properties.

For the present analysis, the soil is modelled as an isotropic, elastic medium with uniform, isotropic permeabilities. In addition, the effect of the layered media with different permeabilities, is also investigated. The problem is described in Figure 7 showing the point sink at a depth h below the ground surface. Figure 8 depicts the two layered soil with the top and bottom layers having the permeabilities k_1 and k_2, respectively. In all cases, drainage is permitted through the upper half-space surface.

The soil skeleton is assumed to have a Poisson's ratio of 0·25 to be consistent in all comparisons. The axisymmetric boundary element model used for this study requires the discretization of only the surfaces of the layers. The discretization is carried out to a distance of $4h$

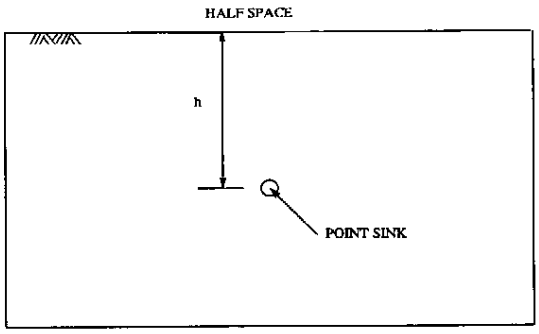

Figure 7. Stresses due to withdrawal of pore fluid — single layer : problem description

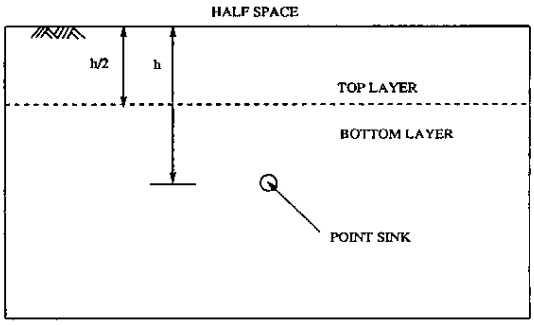

Figure 8. Stresses due to withdrawal of pore fluid — Two layers : problem description

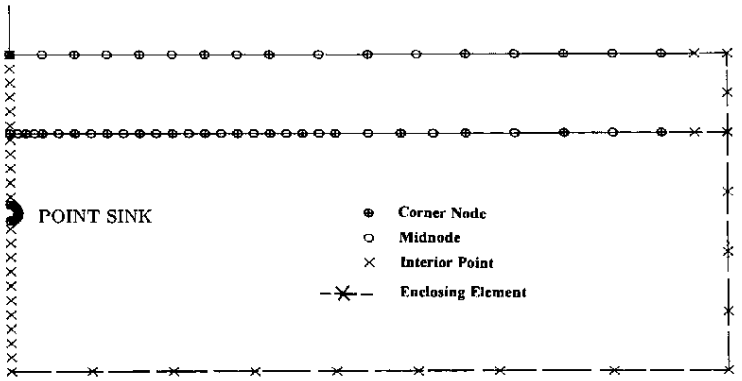

Figure 9. Stresses due to withdrawal of pore fluid — boundary element model

for the transient consolidation analysis of the problem and to a distance of $20h$ for the steady-state analysis. The mesh was truncated after these distances on the basis of convergence studies with various meshes. More refinement in the model is provided to the half-space closer to the sink and enclosing elements[19] are used to model the infinite half-space. The two-layer axisymmetric BEM mesh is shown in Figure 9. The point sink is modelled as a sphere with small but finite radius to allow the imposition of the boundary conditions for flux. The semi-circular axisymmetric section representing the sphere is modelled using four elements.

The pore fluid involved in this pumping process may be compressible in nature. To account for the compressibility of the fluid, a relative compressibility ratio, M/K, is defined, where M is the bulk modulus of pore fluid after adjustment for porosity and K is the bulk modulus of the solid skeleton. The two values of the M/K used in the present analysis are 1·0 and ∞ and the corresponding values for the undrained Poisson's ratio, ν_u, are found to be 0·3636 and 0·5, respectively.

Figure 10 shows the isochrones of excess pore pressure for two sets of non-dimensional times $c_v t/h^2$, where c_v is the coefficient of consolidation of the soil and t is the elapsed time after the start of the pumping process. The negative values of p indicate suction. It was observed by Booker and Carter[3] that if the pore pressure is normalized in the manner shown in Figure 10, then the

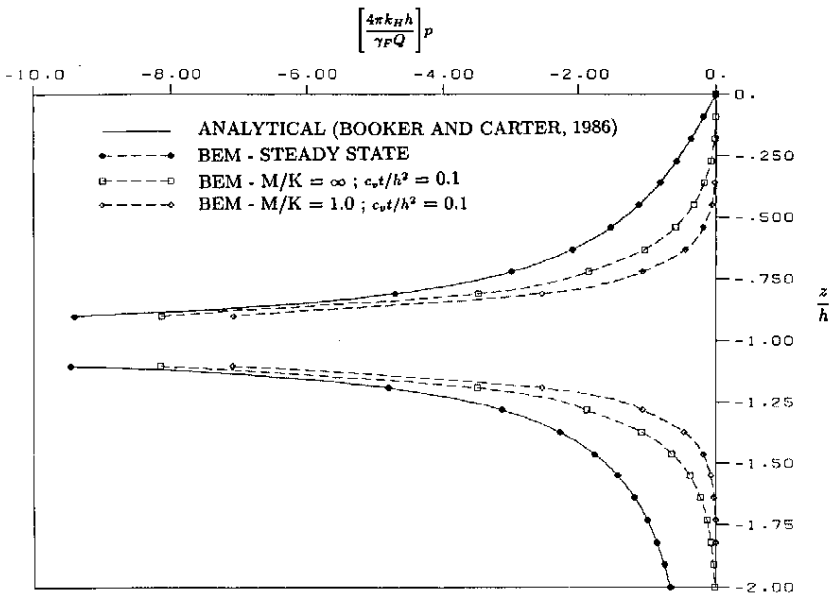

Figure 10. Variation of excess pore pressure with depth

steady-state response (at $c_v t/h^2 = \infty$) is independent of the relative compressibility. A closed-form expression for the excess pore pressure distribution along the axis $r = 0$, for an isotropically permeable soil (i.e. $k_H = k_v = k$) was presented by the above authors as follows:

$$p = -\left(\frac{Q\gamma_F}{4\pi k}\right)\left[\frac{1}{|z+h|} - \frac{1}{|z-h|}\right]$$

where Q is the total flux across the sink (i.e. $4\pi R^2 q$), q is the flux per unit area, γ_F is the unit weight of the pore fluid and k is the permeability.

It can be observed from Figure 10 that the predicted results from the present BEM analysis are in excellent agreement with the analytical results[2] for the steady state ($c_v t/h^2 = \infty$). The isochrones of pore pressure at an intermediate time ($c_v t/h^2 = 0{\cdot}1$) are also plotted. These are now functions of the relative compressibility M/K and the two curves from the present BEM analysis corresponding to the M/K value of 1·0 and ∞ are also shown in the figure. To avoid excessive data presentation on a single figure, the results of Booker and Carter[3] for the transient case are not shown. However, very good agreement was observed for all cases between the predicted and analytical results. These results indicate that the excess pore pressure response is slower for a more compressible fluid, which is consistent with the earlier observations by Booker and Carter.[3]

The changes in effective stresses due to the pumping process are examined next. It must be noted here that negative values of stress indicate compression. The variation of effective radial stress change is plotted with depth in Figure 11 for two stages of the consolidation. The solid curve displays the stress distribution at steady state while the dashed curves are plotted at $c_v t/h^2 = 0{\cdot}1$ for $M/K = 1{\cdot}0$ and ∞. The effective radial stress is normalized in a manner similar to the pore pressure (Figure 10). As evident from the curves, the change in radial stress is non-zero at the surface of the soil and has a very high value close to the sink. In addition, the stress build-up is slower for the more compressible case. Figure 12 depicts the variation of effective radial stress

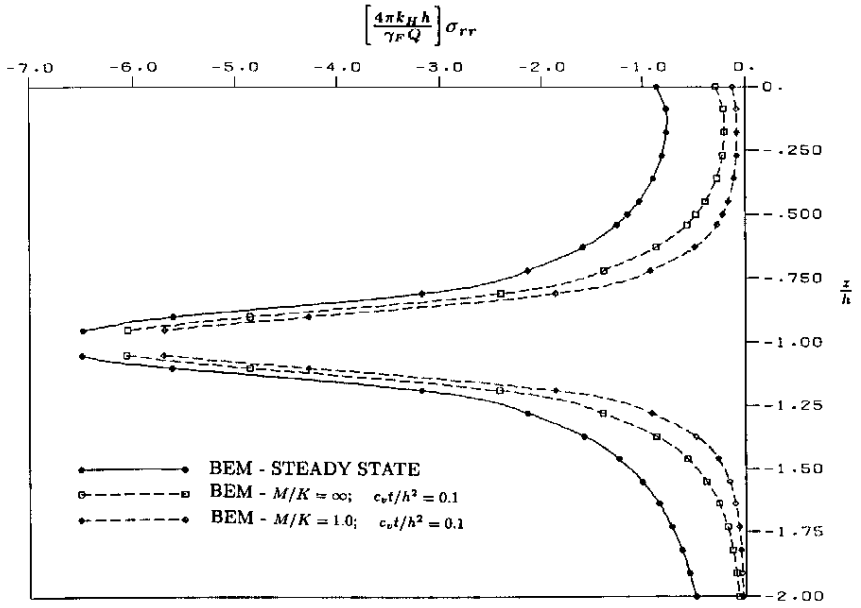

Figure 11. Variation of effective radial stress with depth at three stages of consolidation

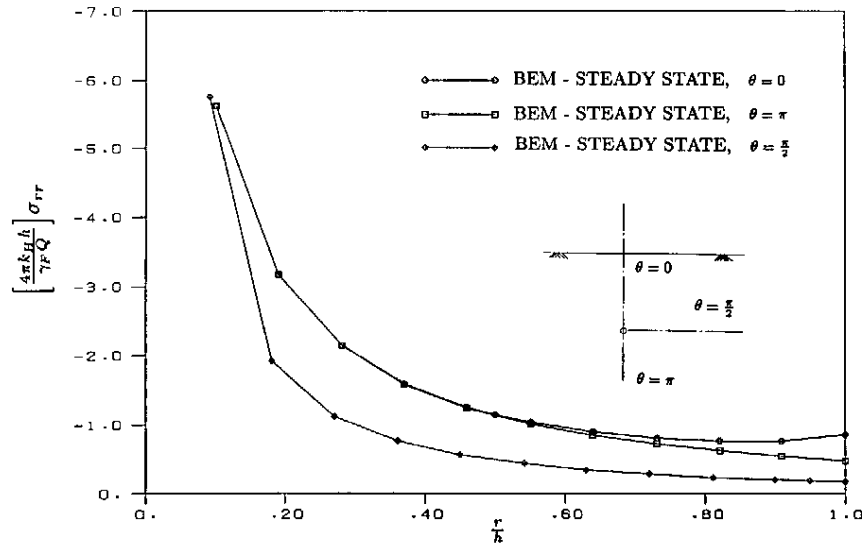

Figure 12. Variation of effective radial stress with radial distance in three different directions from the centre of the sink

change at steady state with outwardly radiating distance in three directions from the centre of the sink. This illustrates the effect of the half-space where the horizontal variation ($\theta = \pi/2$) is significantly different from the vertical ($\theta = 0, \pi$).

The effective axial stress variation with depth is shown in Figure 13 and the dependence of the effective axial stress on the three directions, is shown in Figure 14. It is interesting to note that the

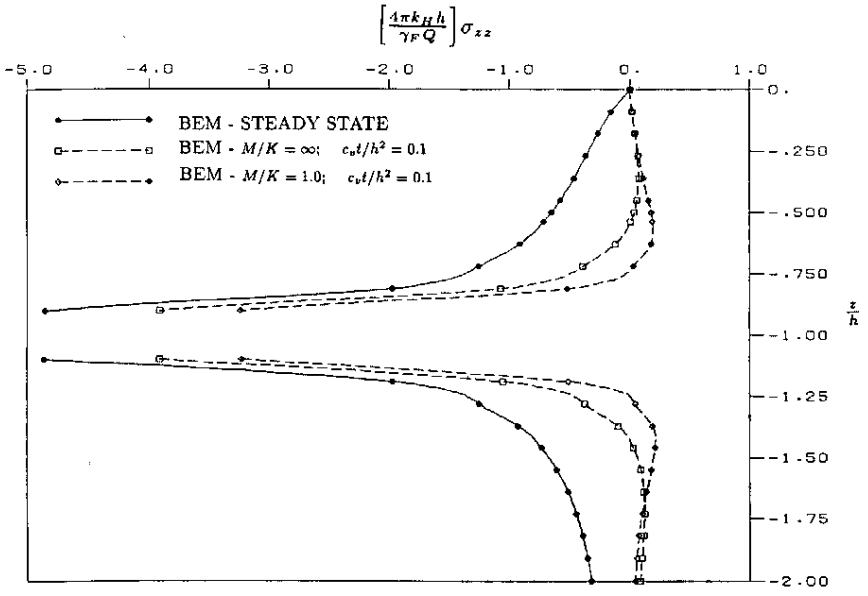

Figure 13. Variation of effective axial stress with depth at three stages of consolidation

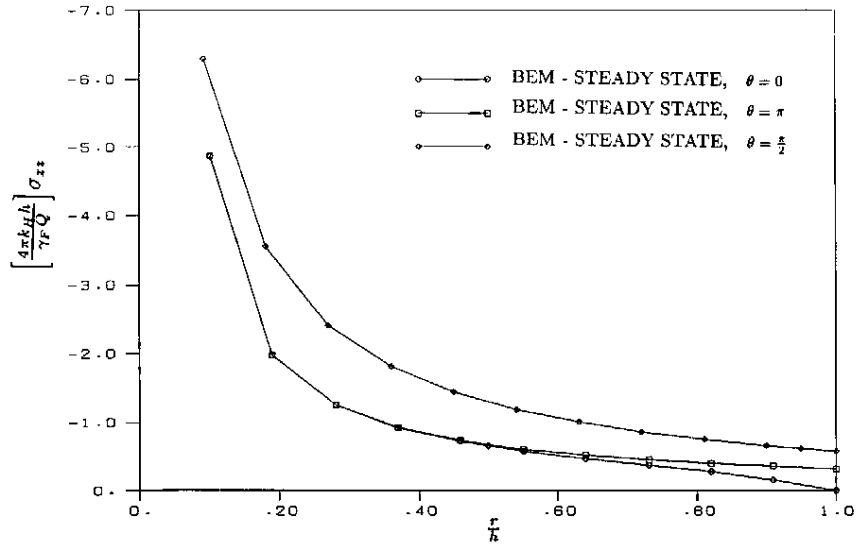

Figure 14. Variation of effective axial stress with radial distance in three different directions from the centre of the sink

effective axial stress is initially tensile at short times before ultimately adopting a compressive nature at steady state.

Lastly, for the case of two-layered soil, Figure 15 depicts the excess pore pressure isochrones at steady state. The permeability of the top layer is k_1 and the bottom layer k_2. Three cases are

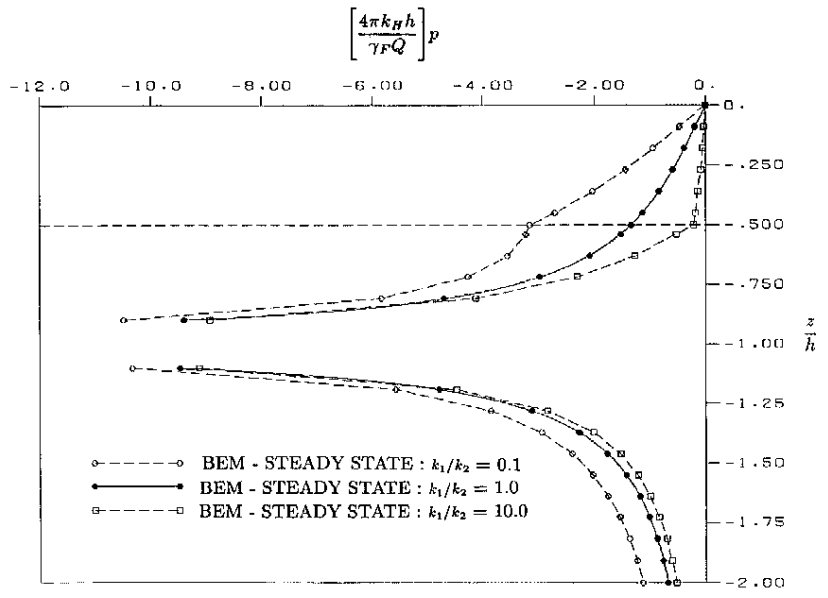

Figure 15. Excess pore pressure isochrones at steady state for three ratios of permeabilities in a two-layered soil

shown in the figure corresponding to three values of the ratio k_1/k_2 as 0·1, 1·0 and 10·0. The first curve (i.e. $k_1/k_2 = 0{\cdot}1$) shows a higher suction value in the top layer as compared to the single-layer case because of its lower permeability. On the other hand, the third curve (i.e. $k_1/k_2 = 10{\cdot}0$) exhibits the opposite trend. However, the response at depths away from the interface remains more or less unchanged.

CONCLUSIONS

A linear, axisymmetric time-domain BEM formulation for the evaluation of stresses in a soil mass undergoing consolidation under quasistatic conditions, has been developed in this paper. The present formulation is based on a previous work for displacement calculations and extends its scope to handle stress computations. It still involves only surface variables through the use of infinite space fundamental solutions. The spatial discretization only requires the modelling of the generator of axisymmetric bodies. The stress integral equations are derived from the corresponding boundary integral equations by differentiation. Starting with the three-dimensional boundary integral formulation, a suitable transformation into a cylindrical co-ordinate system is conducted. By considering purely axisymmetric loading and boundary conditions, the circumferential degree of freedom is removed through integration and the corresponding axisymmetric stress integral equations are developed.

The exact equations are discretized in time and space using suitable numerical schemes. This allows for the analysis of a number of significant practical applications involving complex geometries and time-dependent boundary conditions. Some such practical problems are studied and very accurate solutions are obtained.

APPENDIX

Axisymmetric poroelastic steady-state interior stress kernels

This appendix provides the details of the generalized interior stress kernels for axisymmetric steady-state poroelasticity. These kernels, when used in conjunction with the numerical tangential integration of the transient part of the three-dimensional kernels in the next section, produce a complete set for quasistatic axisymmetric analysis. The following generalized notation is employed:

$X = x_i = \{R \;\; Z\}^{\mathrm{T}}$ co-ordinates of integration point of ring source

$\xi = \xi_i = \{r \;\; z\}^{\mathrm{T}}$ co-ordinates of field point

$n_r(R, Z)$ normal in r direction at integration point

$n_z(R, Z)$ normal in z direction at integration point

The indices i, j assume the values 1 and 2 only or, equivalently r and z. The index p refers to the pore pressure component in the third position of the generalized displacement or traction vector. Thus, for example, u_{p} is the pore pressure while t_{p} represents the flux. The Greek indices α, β vary from 1 to 3.

The steady-state interior stress axisymmetric kernels for poroelasticity are presented below. The elastostatic portion of these kernels is identical to the kernels described in Henry *et al.*[18] and is provided below for completeness. Thus, in the stress equation (12), the steady-state kernels $\hat{G}^{\sigma}_{ijk}$ and $\hat{F}^{\sigma}_{ijk}$ are given by the relationships ($i = r, z$)

$$\hat{G}^{\sigma}_{irr} = c_1 \frac{\partial \hat{G}_{ir}}{\partial r} + c_2 \left(\frac{\hat{G}_{ir}}{r} + \frac{\partial \hat{G}_{iz}}{\partial z} \right)$$

$$\hat{G}^{\sigma}_{izz} = c_1 \frac{\partial \hat{G}_{iz}}{\partial z} + c_2 \left(\frac{\hat{G}_{ir}}{r} + \frac{\partial \hat{G}_{iz}}{\partial r} \right)$$

$$\hat{G}^{\sigma}_{irz} = \mu \left(\frac{\partial \hat{G}_{iz}}{\partial r} + \frac{\partial \hat{G}_{ir}}{\partial z} \right)$$

$$\hat{G}^{\sigma}_{i\theta\theta} = c_1 \left(\frac{\hat{G}_{ir}}{r} \right) + c_2 \left(\frac{\partial \hat{G}_{ir}}{\partial r} + \frac{\partial \hat{G}_{iz}}{\partial z} \right)$$

and

$$\hat{F}^{\sigma}_{irr} = c_1 \frac{\partial \hat{F}_{ir}}{\partial r} + c_2 \left(\frac{\hat{F}_{ir}}{r} + \frac{\partial \hat{F}_{iz}}{\partial z} \right)$$

$$\hat{F}^{\sigma}_{izz} = c_1 \frac{\partial \hat{F}_{iz}}{\partial z} + c_2 \left(\frac{\hat{F}_{ir}}{r} + \frac{\partial \hat{F}_{iz}}{\partial r} \right)$$

$$\hat{F}^{\sigma}_{irz} = \mu \left(\frac{\partial \hat{F}_{iz}}{\partial r} + \frac{\partial \hat{F}_{ir}}{\partial z} \right)$$

$$\hat{F}^{\sigma}_{i\theta\theta} = c_1 \left(\frac{\hat{F}_{ir}}{r} \right) + c_2 \left(\frac{\partial \hat{F}_{ir}}{\partial r} + \frac{\partial \hat{F}_{iz}}{\partial z} \right)$$

where

$$\frac{\partial \hat{G}_{ij}}{\partial r} = \frac{\partial A_{ij}}{\partial r} K(m) + \frac{\partial B_{ij}}{\partial r} E(m) + A_{ij} \frac{\partial K}{\partial r} + B_{ij} \frac{\partial E}{\partial r}$$

$$\frac{\partial \hat{G}_{ij}}{\partial z} = -\frac{\partial \hat{G}_{ij}}{\partial Z}, \quad i,j = r,z$$

$$\frac{\partial \hat{F}_{ri}}{\partial r} = \left[c_1 \frac{\partial^2 \hat{G}_{ri}}{\partial R \partial r} + c_2 \left(\frac{1}{R} \frac{\partial \hat{G}_{ri}}{\partial r} + \frac{\partial^2 \hat{G}_{zi}}{\partial Z \partial r} \right) \right] n_r + \mu \left(\frac{\partial^2 \hat{G}_{ri}}{\partial Z \partial r} + \frac{\partial^2 \hat{G}_{zi}}{\partial R \partial r} \right) n_z, \quad i = r,z$$

and similar expressions for $\partial \hat{F}_{ri}/\partial z$, $\partial \hat{F}_{zi}/\partial r$ and $\partial \hat{F}_{zi}/\partial z$. The constants c_1 and c_2 are given by

$$c_1 = \frac{E(1-\nu)}{(1+\nu)(1-2\nu)}$$

$$c_2 = \frac{E\nu}{(1+\nu)(1-2\nu)}$$

and $K(m)$ is the complete elliptic integral of the first kind and $E(m)$ is the complete elliptic integral of the second kind.

The second-order partial derivative terms in the above equations may be expressed as

$$\frac{\partial^2 \hat{G}_{ij}}{\partial R \partial r} = \frac{\partial^2 A_{ij}}{\partial R \partial r} K + \frac{\partial A_{ij}}{\partial R} \frac{\partial K}{\partial r} + \frac{\partial A_{ij}}{\partial r} \frac{\partial K}{\partial R} + A_{ij} \frac{\partial^2 K}{\partial R \partial r}$$
$$+ \frac{\partial^2 B_{ij}}{\partial R \partial r} E + \frac{\partial B_{ij}}{\partial R} \frac{\partial E}{\partial r} + \frac{\partial B_{ij}}{\partial r} \frac{\partial E}{\partial R} + B_{ij} \frac{\partial^2 E}{\partial R \partial r}, \quad i = r,z$$

and similarly for $\partial^2 \hat{G}_{ij}/\partial R \partial z$, $\partial^2 \hat{G}_{ij}/\partial Z \partial r$ and $\partial^2 \hat{G}_{ij}/\partial Z \partial z$. The derivatives of $\hat{G}_{ij}$ and $\hat{F}_{ij}$ along with terms involving A_{ij}, B_{ij}, $K(m)$ and $E(m)$ may be obtained easily and are not detailed.

The expressions for the coupling terms of the steady-state kernels $\hat{G}^{\sigma}_{\mathrm{p}ij}$ and $\hat{F}^{\sigma}_{\mathrm{p}ij}$ are identical to $\hat{G}^{\sigma}_{ijk}$ and $\hat{F}^{\sigma}_{ijk}$ above with the first subscript (i) replaced by the subscript (p) for pore pressure.

The corresponding derivatives, in an explicit form, are given by

$$\frac{\partial \hat{G}_{pr}}{\partial r} = -\frac{M}{r^2 H} a_2 K(m) + \left[\frac{N^2}{r^2 H \rho^2} + \frac{2\bar{Z}^2}{H\rho^2} \right] a_2 E(m)$$

$$\frac{\partial \hat{G}_{pr}}{\partial z} = \left(-\frac{\bar{Z}}{rH} \right) a_2 K(m) + \left(\frac{N\bar{Z}}{rH\rho^2} \right) a_2 E(m)$$

$$\frac{\partial \hat{G}_{pz}}{\partial z} = \left(-\frac{\bar{Z}}{rH} \right) a_2 K(m) + \left(\frac{N\bar{Z}}{rH\rho^2} \right) a_2 E(m)$$

$$\frac{\partial \hat{G}_{pz}}{\partial z} = \left(-\frac{2}{H} \right) a_2 K(m) + \left(\frac{2\bar{Z}^2}{H\rho^2} \right) a_2 E(m)$$

and

$$\frac{\partial \hat{F}_{pr}}{\partial z} = \left[\left\{ -\frac{\bar{Z}}{rRH} - \frac{M\bar{Z}^3}{rRH^3\rho^2} \right\} a_2 k K(m) + \left\{ -\frac{\bar{Z}(M+3\bar{Z}^2)}{rRH\rho^2} + \frac{4M^2\bar{Z}^3}{rRH^3\rho^4} \right\} a_2 k E(m) \right] n_r$$
$$+ \left[\left\{ -\frac{1}{rH} - \frac{N\bar{Z}^2}{rH^3\rho^2} \right\} a_2 k K(m) + \left\{ \frac{(N+3\bar{Z}^2)}{rH\rho^2} - \frac{4MN\bar{Z}^2}{rH^3\rho^4} \right\} a_2 k E(m) \right] n_z$$

$$\frac{\partial \hat{F}_{pz}}{\partial z} = \left[\left\{\frac{1}{RH} + \frac{\bar{H}\bar{Z}^2}{RH^3\rho^2}\right\}a_2kK(m) + \left\{\frac{\bar{H} - 3\bar{Z}^2}{RH\rho^2} - \frac{4\bar{H}M\bar{Z}^2}{RH^3\rho^4}\right\}a_2kE(m)\right]n_r$$
$$+ \left[\left\{\frac{2\bar{Z}^3}{H^3\rho^2}\right\}a_2kK(m) + \left\{\frac{6\bar{Z}}{H\rho^2} - \frac{8M\bar{Z}^3}{H^3\rho^4}\right\}a_2kE(m)\right]n_z$$

$$\frac{\partial \hat{F}_{pr}}{\partial r} = \left[\left\{\frac{2}{RH} - \frac{r^2+R^2}{r^2RH} - \frac{(r+R)(r^2+R^2)}{rRH^3} - \frac{(r^2+R^2)N}{2r^2RH^3} - \frac{MN\bar{Z}^2}{2r^2RH^3\rho^2} + \frac{HN}{2r^2RH^2}\right\}a_2kK(m)\right.$$
$$+ \left\{\frac{(r^2+R^2)N}{2r^2RH\rho^2} + \frac{2\bar{Z}^2}{RH\rho^2} - \frac{M\bar{Z}^2}{r^2RH\rho^2} - \frac{M\bar{Z}^2(R+r)}{rRH^3\rho^2} + \frac{2M\bar{Z}^2(R-r)}{rRH\rho^4} + \frac{MNZ^2}{2r^2RH^3\rho^2} + \frac{H}{r^2R}\right.$$
$$\left.\left. - \frac{(R+r)}{rRH} - \frac{HN}{2r^2RH^2}\right\}a_2kE(m)\right]n_r$$
$$+ \left[\left\{-\frac{3\bar{Z}}{2r^2h} + \frac{N^2\bar{Z}}{2r^2H^3\rho^2}\right\}a_2kK(m) + \left\{\frac{3N\bar{Z}}{2r^2H\rho^2} + \frac{2\bar{Z}}{H\rho^2} + \frac{N\bar{Z}(R+r)}{rH^3\rho^2} - \frac{2N\bar{Z}(R-r)}{rH\rho^4}\right.\right.$$
$$\left.\left. - \frac{N^2\bar{Z}}{2r^2H^3\rho^2}\right\}a_2kE(m)\right]n_z$$

$$\frac{\partial \hat{F}_{pz}}{\partial r} = \left[\left\{\frac{\bar{Z}}{rRH} - \frac{M\bar{Z}^3}{rRH^3\rho^2}\right\}a_2kK(m) + \left\{\frac{-\bar{Z}(N-4r^2)}{2rRH\rho^2} - \frac{\bar{H}\bar{Z}(\rho^2-4r^2)}{2rRH^3\rho^2}\right.\right.$$
$$\left.\left. - \frac{2\bar{H}\bar{Z}(R-r)}{RH\rho^4}\right\}a_2kE(m)\right]n_r$$
$$+ \left[\left\{-\frac{1}{rH} + \frac{N\bar{Z}^2}{rH^3\rho^2}\right\}a_2kK(m) + \left\{\frac{N}{rH\rho^2} - \frac{\bar{Z}^2(\rho^2-4r^2)}{rH^3\rho^2} - \frac{4\bar{Z}^2(R-r)}{H\rho^4}\right\}a_2kE(m)\right]n_z.$$

$$\bar{Z} = Z - z, \qquad H^2 = (R+r)^2 + \bar{Z}^2, \qquad \rho^2 = [(R-r)^2 + \bar{Z}^2]$$

$$M = R^2 + r^2 + \bar{Z}^2, \qquad N = R^2 - r^2 + \bar{Z}^2, \qquad \bar{H} = R^2 - r^2 - \bar{Z}^2, \qquad m = \frac{4Rr}{H^2}$$

$$a_1 = \frac{R}{8\pi\mu(1-\nu)} \qquad b_1 = (3 - 4\nu)$$

$$a_2 = \frac{R\beta}{4\pi k(\lambda + 2\mu)}, \qquad a_3 = \frac{R}{2\pi k}$$

$$\frac{\partial K}{\partial R} = \frac{(M - 2R^2)P}{2R}, \qquad \frac{\partial E}{\partial R} = -\frac{(M - 2R^2)Q}{2RH^2}$$

$$\frac{\partial K}{\partial Z} = -\bar{Z}P, \qquad \frac{\partial E}{\partial Z} = \frac{\bar{Z}}{H^2}Q$$

$$P = \frac{E}{\rho^2} - \frac{K}{H^2}, \qquad Q = K - E$$

Three-dimensional transient interior stress kernels

This appendix contains the details of all the transient kernel functions utilized in the poroelastic boundary element formulation. These three-dimensional kernels are based upon continuous

source and force fundamental solutions. The poroelastic theory is unconditionally fully coupled and the entire coupled three-dimensional kernel must be considered, as shown below. The following relationships must be used to determine the proper form of the functions required in the boundary clement discretization, that is,

$$G^{n}_{\beta\alpha}(X;\xi) = g^{\mathrm{tr}}_{\beta\alpha}(X;\xi,n\Delta\tau) \quad \text{for } n=1$$

$$G^{n}_{\beta\alpha}(X;\xi) = g^{\mathrm{tr}}_{\beta\alpha}(X;\xi,n\Delta\tau) - g^{\mathrm{tr}}_{\beta\alpha}(X;\xi,(n-1)\Delta\tau) \quad \text{for } n>1,$$

$$G^{\sigma;n}_{\beta ij}(X;\xi) = {}^{\mathrm{tr}}g^{\sigma}_{\beta ij}(X;\xi,n\Delta\tau) \quad \text{for } n=1$$

$$G^{\sigma;n}_{\beta ij}(X;\xi) = {}^{\mathrm{tr}}g^{\sigma}_{\beta ij}(X;\xi,n\Delta\tau) - {}^{\mathrm{tr}}g^{\sigma}_{\beta ij}(X;\xi,(n-1)\Delta\tau) \quad \text{for } n>1,$$

with similar expressions holding for the remaining kernels. In the specification of these kernels below, the arguments $(X;\xi,\tau)$ are assumed.

The indices i,j,k,l vary from 1 to 3, α,β vary from 1 to 4 and p equals 4.

Additionally, x_i are the co-ordinates of integration point, ξ_i are the co-ordinates of field point, $y_i = x_i - \xi_i$, $r^2 = y_i y_i$, $\eta = r/(c_v\tau)^{1/2}$ and $c_1 = (\nu_u - \nu)/(1-\nu_u)$.

Boundary kernels. For the generalized transient displacement kernel,

$$g^{\mathrm{tr}}_{ij} = \frac{1}{16\pi r}\frac{1}{\mu(1-\nu)}\left[\left(\frac{y_i - y_j}{r^2}\right)g_1(\eta) + (\delta_{ij})g_2(\eta)\right]$$

$$g^{\mathrm{tr}}_{ip} = \frac{1}{4\pi}\left(\frac{\beta}{\kappa(\lambda+2\mu)}\right)\left[\left(\frac{y_i}{r}\right)g_3(\eta)\right]$$

$$g^{\mathrm{tr}}_{pj} = \frac{1}{8\pi}\left(\frac{\beta}{\kappa(\lambda+2\mu)}\right)\left[\left(\frac{y_j}{r}\right)g_4(\eta)\right]$$

$$g^{\mathrm{tr}}_{pp} = \frac{1}{4\pi r}\left(\frac{1}{\kappa}\right)[g_5(\eta)]$$

whereas, for the generalized transient traction kernel,

$$f^{\mathrm{tr}}_{ij} = \frac{1}{8\pi r^2}\frac{1}{1-\nu}\left[-\left(\frac{y_i y_j y_k n_k}{r^3}\right)f_1(\eta) - \left(\frac{\delta_{ij}y_k n_k + y_i n_j}{r}\right)f_2(\eta) + \left(\frac{y_j n_i}{r}\right)f_3(\eta)\right]$$

$$f^{\mathrm{tr}}_{ip} = \frac{1}{2\pi r}\left(\frac{\mu\beta}{\kappa(\lambda+2\mu)}\right)\left[\left(\frac{y_i y_k n_k}{r^2}\right)f_4(\eta) + (n_i)f_5(\eta)\right)$$

$$f^{\mathrm{tr}}_{pj} = \frac{1}{8\pi r}\left(\frac{\beta}{\lambda+2\mu}\right)\left[\left(\frac{y_i y_k n_k}{r^2}\right)f_6(\eta) - (n_j)f_7(\eta)\right]$$

$$f^{\mathrm{tr}}_{pp} = \frac{1}{4\pi r^2}\left[\left(\frac{y_k n_k}{r}\right)f_8(\eta)\right]$$

In the above,

$$\mathrm{erf}(z) = \frac{2}{\sqrt{\pi}}\int_0^z \mathrm{e}^{-x^2}\,\mathrm{d}x$$

$$h_1(\eta) = \mathrm{erf}\left(\frac{\eta}{2}\right) - \frac{\eta}{\sqrt{\pi}}\mathrm{e}^{-\eta^2/4}, \qquad h_1' = \frac{\partial h_1}{\partial \eta}$$

$$h_2(\eta) = \frac{6h_1(\eta)}{\eta^2} - \frac{\eta}{\sqrt{\pi}} e^{-\eta^2/4}$$

$$g_1(\eta) = c_1\{h_1(\eta) - h_2(\eta)\}$$

$$g_2(\eta) = -c_1\left\{h_1(\eta) - \frac{h_2(\eta)}{3} + \frac{2\eta}{3\sqrt{\pi}} e^{-\eta^2/4}\right\}$$

$$g_3(\eta) = \frac{h_1(\eta)}{\eta^2 t}$$

$$g_4(\eta) = -\operatorname{erf}\left(\frac{\eta}{2}\right) + \frac{2h_1(\eta)}{\eta^2}$$

$$g_5(\eta) = -\operatorname{erf}\left(\frac{\eta}{2}\right)$$

$$f_1(\eta) = 3c_1\left\{h_1 - \frac{5h_2}{3}\right\}$$

$$f_2(\eta) = -c_1\{h_1 - h_2\}$$

$$f_3(\eta) = c_1\{h_1 + h_2\}$$

$$f_4(\eta) = \frac{h_1'}{\eta t} - \frac{3h_1}{\eta^2 t}$$

$$f_5(\eta) = \frac{h_1(\eta)}{\eta^2 t} - \frac{h_1'}{\eta t}$$

$$f_6(\eta) = -\operatorname{erf}\left(\frac{\eta}{2}\right) + \frac{6h_1(\eta)}{\eta^2}$$

$$f_7(\eta) = -\operatorname{erf}\left(\frac{\eta}{2}\right) + \frac{2h_1(\eta)}{\eta^2}$$

$$f_8(\eta) = -h_1(\eta).$$

Interior effective stress kernels. The transient portion of the three-dimensional interior effective stress kernels for soil consolidation are provided below:

$${}^{tr}g^{\sigma}_{\beta ij} = \frac{2\mu\nu}{1-2\nu}\delta_{ij}\frac{\partial g^{tr}_{\beta l}}{\partial \xi_l} + \mu\left(\frac{\partial g^{tr}_{\beta i}}{\partial \xi_j} + \frac{\partial g^{tr}_{\beta j}}{\partial \xi_i}\right)$$

$${}^{tr}f^{\sigma}_{\beta ij} = \frac{2\mu\nu}{1-2\nu}\delta_{ij}\frac{\partial f^{tr}_{\beta l}}{\partial \xi_l} + \mu\left(\frac{\partial f^{tr}_{\beta i}}{\partial \xi_j} + \frac{\partial f^{tr}_{\beta j}}{\partial \xi_i}\right)$$

where

$$\frac{\partial g^{tr}_{ij}}{\partial \xi_k} = \frac{1}{16\pi r^2}\frac{1}{\mu(1-\nu)}\left[\left(\frac{3y_iy_jy_k}{r^3} - \frac{\delta_{jk}y_i}{r} - \frac{\delta_{ik}y_i}{r}\right)c_1(h_1 + h_2)\right.$$
$$\left. - \left(\frac{\partial_{ij}y_k}{r}\right)c_1\left(h_1 - \frac{h_2}{3} + \frac{2\eta}{3\sqrt{\pi}}e^{-\eta^2/4}\right) - \left(\frac{y_iy_jy_k}{r^3}\right)\eta g_1' - \left(\frac{\delta_{ij}y_k}{r}\right)\eta g_2'\right]$$

$$\frac{\partial g_{pj}^{tr}}{\partial \xi_k} = \frac{1}{8\pi r}\left(\frac{\beta}{k(\lambda+2\mu)}\right)\left[\left(\frac{y_j y_k}{r^2} - \delta_{jk}\right)g_4 - \left(\frac{y_j y_k}{r^2}\right)\eta g_4'\right]$$

$$\frac{\partial f_{ij}^{tr}}{\partial \xi_k} = \frac{1}{8\pi r^3}\frac{1}{(1-\nu)}\left[-\left(\frac{5y_i y_j y_k y_l n_l}{r^4} - \frac{y_i y_j n_k}{r^2} - \frac{\delta_{jk} y_i y_l n_l}{r^2} - \frac{\delta_{ij} y_j y_l n_l}{r^2}\right)3c_1\left(h_1 - \frac{5h_2}{3}\right)\right.$$
$$-\left(\frac{3\delta_{ij} y_k y_l n_l}{r^2} - \delta_{ij} n_k + \frac{3y_i y_k n_j}{r^2} - \delta_{ik} n_j\right)c_1(h_2 - h_1) - \left(\frac{3y_j y_k n_i}{r^2} - \delta_{jk} n_i\right)c_1(h_1 + h_2)$$
$$\left. + \left(\frac{y_i y_j y_k y_l n_l}{r^4}\right)\eta f_1' + \left(\frac{\delta_{ij} y_k y_l n_l + y_i y_k n_j}{r^2}\right)\eta f_2' - \left(\frac{y_j y_k n_i}{r^2}\right)\eta f_3'\right]$$

$$\frac{\partial f_{pj}^{tr}}{\partial \xi_k} = \frac{1}{8\pi r^2}\left(\frac{\beta}{\lambda+2\mu}\right)\left[\left(\frac{3y_j y_k y_l n_l}{r^3} - \frac{y_j n_k}{r} - \frac{\delta_{jk} y_l n_l}{r}\right)f_6(\eta)\right.$$
$$\left. + \left(\frac{y_k n_j}{r}\right)f_7(\eta) - \left(\frac{y_j y_k y_l n_l}{r^3}\right)\eta f_6' + \left(\frac{y_k n_j}{r}\right)\eta f_7'\right]$$

and the prime, $'$, represents a derivative with respect to η. Hence,

$$g_1' = \frac{\partial g_1(\eta)}{\partial \eta}$$

and so on.

REFERENCES

1. M. A. Biot, 'General theory of three-dimensional consolidation', *J. Appl. Phys.*, **12**, 155–164 (1941).
2. J. R. Booker and J. P. Carter, 'Long term subsidence due to fluid extraction from a saturated, anisotropic, elastic soil mass', *Quart. J. Mech. Appl. Math.*, **39(1)**, 85–97 (1986).
3. J. R. Booker and J. P. Carter, 'Withdrawal of a compressible pore fluid from a point sink in an isotropic elastic half space with anisotropic permeability, *Int. J. Solids Struct.*, **23**, pp. 369–385 (1987).
4. R. S. Sandhu and E. L. Wilson, 'Finite element analysis of seepage in elastic media', *J. eng. mech. div. ASCE*, **95(EM3)**, 641–652 (1969).
5. J. Ghaboussi and E. L. Wilson, 'Flow of compressible fluids in elastic media', *Int. J. numer. methods eng.*, **5**, 419–442 (1973).
6. P. K. Banerjee and R. Butterfield, *Boundary element methods in engineering science*, McGraw-Hill, London, 1981.
7. G. Aramaki and K. Yasuhara, 'Application of the boundary element method for axisymmetric Biot's consolidation', *Eng. Anal.*, **2**, 184–191 (1985).
8. A. H-D. Cheng and J. A. Liggett, 'Boundary integral equation method for linear porous-elasticity with applications to soil consolidation', *Int. j. numer. methods eng.*, **20**, 255–278 (1984).
9. A. H-D. Cheng and J. A. Liggett, 'Boundary integral equation method for linear porous-elasticity with applications to fracture propagation', *Int. j. numer. methods eng.*, **20**, 279–296 (1984).
10. G. F. Dargush and P. K. Banerjee, 'A time domain element method for poroelasticity', *Int. j. numer. methods eng.*, **28**, 2423–2449 (1989).
11. W. Nowacki, 'Green's functions for a thermoelastic medium (quasistatic problems)', *Bull. Inst. Polit. Jasi*, Sierie Noua, **12**(3–4), 83–92 (1966).
12. M. P. Cleary, 'Fundamental solutions for a fluid-saturated porous solid', *Int. J. Solids Struct.*, **13**, 785–806 (1977).
13. J. W. Rudnicki, 'Fluid mass sources and point forces in linear elastic diffusive solids', *Mech. Mater.*, **5**, 383–393 (1987).
14. G. F. Dargush and P. K. Banerjee, 'A boundary element method for axisymmetric soil consolidation', *Int. J. Solids Struct.*, **28**, 897–915 (1991).
15. K. Terzaghi, *Erdbaumechanik auf Bodenphysikalischer Grundlage*, F. Deuticke, Vienna, 1925.
16. J. R. Rice and M. P. Cleary, 'Some basic stress diffusion solutions for fluid-saturated elastic porous media with compressible constituents', *Rev. Geophys. Space Phys.*, **14**, 227–241 (1976).
17. V. Ionescu-Cazimir, 'Problem of linear coupled thermoelasticity. Theorems on reciprocity for the dynamic problem of coupled thermoelasticity, I', *Bull. de l'academie Polonaise des Sciences*, Series des Sciences Techniques, **12**, 473–488 (1964).

18. D. P. Henry, D. A. Pape and P. K. Banerjee, 'New axisymmetric BEM formulation for body forces using particular integrals', *J. eng. mech. ASCE*, **113**, 671–688 (1987).
19. S. Ahmad and P. K. Banerjee, 'Inelastic transient dynamic analysis of three dimensional problems by BEM', *Int. j. numer. methods eng.*, **29**, 371–390 (1988).
20. H. C. Wang and P. K. Banerjee, 'Axisymmetric transient elastodynamic analysis by boundary element method', *Int. J. Solids Struct.*, **26**, 401–415 (1990).
21. T. A. Cruse and W. Vanburen, 'Three-dimensional elastic stress analysis of a fracture specimen with an edge crack', *Int. J. Frac. Mech.*, **7**, 1–15 (1971).
22. F. J. Rizzo and D. J. Shippy, 'An advanced boundary integral equation method for three-dimensional thermoelasticity', *Int. j. numer. methods eng.*, **11**, 1753–1768 (1977).
23. M. A. Biot, 'General solutions of the equations of elasticity and consolidation for a porous material', *J. appl. mech., ASME*, **23**, 91–96 (1956).
24. C. W. Cryer, 'A comparison of the three-dimensional consolidation theories of Biot and Terzaghi', *Quart. J. Mech. Appl. Math.*, **XVI**, 401–411 (1963).
25. N. Makris, G. F. Dargush and M. C. Constantinou, 'Dynamic analysis of generalized viscoelastic fluids', *J. eng. mech., ASCE*, **119**, 1663–1679 (1993).
26. J. C. Small and J. R. Booker, 'Surface deformation of layered soil deposits due to extraction of water', *Proc. 9th Australian Conf. on Mech. Struct. Materials, Sydney*, Australia, 1984, pp. 33–38.
27. J. P. Hsi, J. P. Carter and J. C. Small, 'Pumping-induced land subsidence in a soil with anisotropic permeability', *Proc. 8th Int. Conf. on Comp. Meth. and Advances in Geomechanics*, Morgantown, USA, 1994, pp. 1211–1216.